Thermodynamic Computing via Autonomous Quantum Thermal Machines

Patryk Lipka-Bartosik,[1] Martí Perarnau-Llobet,[1] and Nicolas Brunner[1]

[1]*Department of Applied Physics, University of Geneva, 1211 Geneva, Switzerland*

(Dated: August 31, 2023)

We develop a physics-based model for classical computation based on autonomous quantum thermal machines. These machines consist of few interacting quantum bits (qubits) connected to several environments at different temperatures. Heat flows through the machine are here exploited for computing. The process starts by setting the temperatures of the environments according to the logical input. The machine evolves, eventually reaching a non-equilibrium steady state, from which the output of the computation can be determined via the temperature of an auxilliary finite-size reservoir. Such a machine, which we term a "thermodynamic neuron", can implement any linearly-separable function, and we discuss explicitly the cases of NOT, 3-majority and NOR gates. In turn, we show that a network of thermodynamic neurons can perform any desired function. We discuss the close connection between our model and artificial neurons (perceptrons), and argue that our model provides an alternative physics-based analogue implementation of neural networks, and more generally a platform for thermodynamic computing.

I. INTRODUCTION

Computing systems can take a variety of forms, from biological cells to massive supercomputers, and perform a broad range of tasks, from basic logic operation to machine learning. In all cases, the computational process must adhere to the principles of physics, and, in particular, to the laws of thermodynamics. In general information processing and thermodynamics are deeply connected, see e.g. [1–3].

From a fundamental perspective, the thermodynamic cost of computing is connected to the concept of reversibility. Computational models based on logical operations that are irreversible (e.g. NAND, as in standard computers) must dissipate a minimal amount of heat due to Landauer's principle [4]. Nevertheless, it is in principle possible to perform computations in a fully reversible manner, in which case there is no direct thermodynamic cost [5, 6]. Such models remain however mostly of theoretical interest, as reversible computation can only be implemented extremely slowly and with a perfectly isolated device [7].

More recently, new links between thermodynamics and computation are being developed. At the fundamental level, bounds for the thermodynamic cost of computation have been derived, see e.g. [8–10]. From a more practical perspective, a promising direction explores low-dissipation computing. Here, models for elementary gates and circuits based on electronic transistors working in the mesoscopic regime, or even towards the single-electron mode, are considered [11–17]. A key aspect is to devise models that are thermodynamically consistent, in order to discuss their energetic cost via the framework of stochastic thermodynamics [18]. This approach already brought considerable progress and further insight can be expected by moving to the fully quantum regime [19–23].

Another exciting direction is thermodynamic computing [24, 25]. This represents a new paradigm for alternative physics-based models of computation, similarly to quantum computing or DNA computing. The main idea is to exploit the thermodynamic behaviour of complex, non-equilibrium physical systems to perform computations, looking for a computational speed-up but also a reduced energy cost. This approach
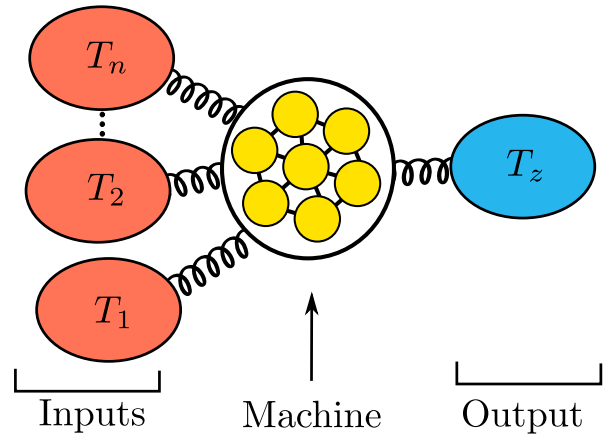

FIG. 1. **Thermodynamic neuron.** The thermodynamic neuron is an autonomous quantum thermal machine designed for computing. The device consists of few interacting qubits (yellow dots), connected to several thermal environments. The input of the computation is encoded in the temperature of heat baths (depicted in red). This generates heat flows through the machine, which eventually reaches a non-equilibrium steady state. The output of the computation can be retrieved from the final temperature of a finite-size reservoir (shown in blue). By designing the machine (setting the qubit energies and their interaction), specific functions between the input and output temperatures can be implemented.

has been explored in the context of machine learning and AI, see e.g. [26–29]. Very recently, promising progress has been reported, showing that a computational speedup in linear algebra problems can be achieved via a controllable system of coupled harmonic oscillators embedded in a thermal bath [30].

In this work, we develop a model for thermodynamic computing starting from a minimal model of a quantum thermal machine. More precisely, we develop autonomous quantum thermal machines that can operate as computing devices where logical inputs and outputs are encoded in the temperature. As our device shares strong similarities with the basic model of an artificial neuron (the perceptron used e.g. in neural networks), we refer to it as a "thermodynamic neuron". Overall, our guiding motivation is to use diverse techniques

offered by quantum thermodynamics to enhance our understanding of fundamental aspects of computation.

To construct our computing device, we start from the model of minimal autonomous quantum thermal machines [31, 32], which are made of a small quantum system (few interacting qubits) in contact with thermal baths at different temperatures. A first observation is that the effect of such a thermal machine onto an external system—heating or cooling—depends on the temperatures of the heat baths. Viewing these temperatures as an input, and the temperature of the external system as an output, the thermal machine can be seen as a computing device (see Fig. 1). By associating a logical value to the temperature (e.g. cold temperatures corresponding to logical "0" and hot temperatures to logical "1"), we show that the autonomous machine can implement logical gates. As a first example, we show how a small quantum refrigerator/heat pump can be used to implement an inverter (NOT gate). This represents the simplest example of a thermodynamic neuron. In turn, we present a general model of a thermodynamic neuron, and show that it can implement any linearly-separable function. We discuss explicitly the examples of NOR and 3-majority. A key element in this construction are the concepts of virtual qubits and virtual temperatures [32], which allow us to establish a close connection between our machines and perceptrons, a common model of an artificial neuron. Furthermore, we show that by constructing networks of thermodynamic neurons, one can implement any desired function, and we discuss the example of XOR. We detail an algorithm, inspired by artificial neural networks, for designing thermodynamic neurons (and networks of them) for implementing any given target function. We conclude with a discussion and an outlook.

Before proceeding, we highlight a number of relevant features of our model. First, as it is constructed from a minimal model of quantum thermal machines, the model is thermodynamically consistent. Hence the model allows for an investigation of the trade-off between consumed energy, dissipation and performance, which we investigate. Second, as it is based on changes of temperatures and flows of energy, the model involves only one conserved quantity, namely energy. This is in contrast to other models, in particular models for nano-scale electronic circuits, which typically require at least two conserved quantities (e.g. energy and particle number). Another interesting difference with standard models of computation is that our thermodynamic neurons directly implement logic gates and are not based on building blocks such as transistors. Finally, the functioning of our model can be intuitively understood by exploiting interesting connections between quantum systems at thermal equilibrium and artificial neural networks.

II. AUTONOMOUS QUANTUM THERMAL MACHINES

Quantum thermal machines usually consists of a small-scale physical system described within quantum theory. This system is then placed in contact with external resources, such as thermal baths or driving, in order to implement a thermodynamic task such as cooling, heating or producing work; see e.g. [33] or [34] for reviews.

Here our focus is on a special class of quantum thermal machines known as autonomous quantum thermal machines (see [35] for recent reviews). Their main interest resides in the fact that these machines work autonomously, in the sense that they are powered by external resources that thermal (typically two or more heat baths at different temperatures) and their internal dynamics is time-independent (modeled via a time-independent Hamiltonian). While first models can be traced back to the thermodynamic analysis of masers [36], recent works have developed a framework for discussing minimal models of autonomous thermal machines, working as refrigerators, heat pumps and heat engines [31, 32, 37]. Interestingly many physical models of quantum thermal machines [38–43] can be mapped back to these minimal abstract models [35]. More recently, autonomous machines have also been devised for achieving other tasks such as the creation of entanglement [44], time-keeping (i.e. clocks) [45–47] and thermometry [48]. A key aspect of these machines is their autonomy making them relevant from a practical perspective [49], and first proof-of-principle experiments have been reported [50, 51]. More generally, the limits of designing autonomous quantum devices have been discussed [52].

A. Open quantum system dynamics

In this work, we will focus on autonomous quantum thermal machines consisting of few *qubits*, i.e few two-level quantum systems. To start with, let us review the dynamics of a single qubit in contact with a heat bath. First, the qubit features two energy eigenstates: the ground state $|0\rangle$ and the excited state $|1\rangle$, with respective energies E_0 and $E_1 > E_0$. The state of the qubit is represented by a density operator ρ, and its mean energy is given by $\mathrm{Tr}[\rho H]$, where $H = E_0 |0\rangle\langle 0| + E_1 |1\rangle\langle 1|$ denotes the Hamiltonian. A convenient quantity is the energy gap, $\epsilon := E_1 - E_0$. Without loss of generality we take $E_0 = 0$, so that the qubit's energy is fully specified by its energy gap. When placed in contact with an environment, the qubit evolution is described by the *master equation*:

$$\dot{\rho} = -i[H, \rho] + \mathcal{L}[\rho]. \tag{1}$$

The first term captures the unitary evolution governed by the Hamiltonian, while the second term captures the environment's impact on the qubit via the dissipator $\mathcal{L}[\cdot]$. Here we use the common assumption of weak coupling to write down the dissipator, i.e. we assume that the qubit is weakly correlated with its environment.

As the qubit evolves over time, it eventually reaches a steady-state when $\dot{\rho} = 0$. When the environment is a thermal bath, with an inverse temperature $\beta = 1/kT$, the resulting steady-state is given by a qubit thermal (Gibbs) state: $\tau(\beta) = e^{-\beta H}/Z$, where $Z = \mathrm{tr}\, e^{-\beta H}$ is the canonical partition function. In this case, the probability of the qubit to be in the excited state is given by the Fermi-Dirac distribution

$$g(\beta\epsilon) = \langle 1|\tau(\beta)|1\rangle = \frac{1}{1 + e^{\beta\epsilon}}. \tag{2}$$

Note that this function coincides with the sigmoid function used in machine learning. We will explore this connection more carefully later.

B.   Thermal machines

The machines we will consider typically consist of several qubits, with energy gaps ϵ_k. The qubits weakly interact with each other, via an energy-preserving interaction. This is modeled by a time-independent interaction Hamiltonion, H_{int}, which commutes with the free Hamiltonian $H_0 = \sum_k \epsilon_k |1\rangle\langle 1|_k$, i.e. $[H_{\text{int}}, H_0] = 0$. Each qubit is then connected to a thermal bath. In general these baths are at different (inverse) temperatures β_k. In the regime of weak coupling, the dynamics of such a machine is well captured by a local master equation [53] of the form

$$\dot{\rho} = -i[H_0 + H_{\text{int}}, \rho] + \sum_k \mathcal{L}^{(k)}[\rho_k]. \qquad (3)$$

where ρ now denotes the multi-qubit state of the machine.

For simplicity we use here the so-called *reset model* (see e.g. [31]) in which the dissipators take the simple form

$$\mathcal{L}^{(k)}[\rho] = \gamma_k \left(\text{Tr}_k[\rho] \otimes \tau(\beta_k) - \rho \right), \qquad (4)$$

where γ_k is the coupling, which corresponds to the probability that qubit k thermalizes with its bath. Note that $\text{Tr}_k[\rho]\otimes\tau(\beta_k)$ represents the multi-qubit state after such a thermalization event. This model can be viewed as a collisional process, where in each instant of time the qubit has a certain probability to collision with a thermal qubit from the bath.

A quantity relevant to our analysis is the heat current released in this process. This is given by

$$j_k := \text{Tr}[H\mathcal{L}^{(k)}[\rho]] = \gamma_k \epsilon_k \left[g(\beta_k \epsilon_k) - p_k \right], \qquad (5)$$

where p_k is the probability that the qubit connected to the bath is in an excited state. We note that in certain cases, a qubit of the machine will be coupled to two different baths, in general at different temperatures. In this case, the total dissipators for the qubit is simply obtained by summing the dissipators with respect to each bath. In turn, this implies that the total heat current is the sum of the heat currents with respect to each bath.

Finally, a quantity of interest for our work is the dissipation generated by the machines. To quantify dissipation, we use the so-called entropy production $\dot{\Sigma}$. This quantity captures the fundamental irreversibility of the machine. The second law of thermodynamics restricts the behavior of any thermal machine. For our autonomous machines it reads

$$\dot{\Sigma} := \dot{S}(\rho(t)) - \sum_k \beta_k j_k(t) \geq 0, \qquad (6)$$

where $S(\rho) := -\text{Tr}[\rho \log \rho]$ is the von Neumann entropy of the machine and $j_k(t)$ is the total heat current flowing into the k-th heat bath at time t.

The quantity $\dot{\Sigma}$ is the rate of *entropy production* which quantifies the speed at which heat (entropy) is dumped into all environments connected with the machine, see e.g. [33, 54, 55]. It therefore measures the amount of information that is lost (i.e. transferred to unobserved degrees of freedom). It is also a central quantity appearing in thermodynamic uncertainty relations (TURs) [56–58], as well as bounds on the speed of a stochastic evolution [59].

III.   THERMODYNAMIC NEURON FOR NOT GATE

In this section we describe an autonomous thermal machine implementing an inverter (NOT gate). This represents the simplest example of a thermodynamic neuron. Before moving to a detailed discussion of the device and its functioning, we start by giving a short and intuitive description.

The machine is sketched in Fig. 2a. It is composed of two parts, which we refer to as the *collector* ($\mathcal{C}$) and the *modulator* ($\mathcal{M}$). The collector consists of three interacting qubits connected to different environments (see Fig. 2a). The first two qubits (denoted $\mathcal{C}_0$ and $\mathcal{C}_1$) are connected to two heat baths denoted $\mathcal{B}_0$ and $\mathcal{B}_1$, at inverse temperatures β_0 and β_1 respectively. The first bath $\mathcal{B}_0$ simply represents a reference bath, hence β_0 will simply be fixed to a certain value and called the *reference temperature*. The second bath $\mathcal{B}_1$ will be used to encode the input of the computation. These two heat baths are supposed to have an infinitely large heat capacity, hence their temperature will remain constant during the time evolution of the machine. Finally, the third qubit of the collector (denoted $\mathcal{C}_z$) is connected to an environment $\mathcal{B}_z$ with a finite heat capacity C (this can be viewed as a finite-size reservoir). They key point is that the temperature of $\mathcal{B}_z$ (we denote β_z the inverse temperature) will evolve in time, and the final temperature (in the steady-state regime) will encode the output of the computation.

To guide intuition, it is useful to think of the collector as a simple (three-qubit) thermal machine [31, 32]. When the input temperature is hot ($\beta_1 \ll 1$) the machine works as a refrigerator, i.e. cooling down the output environment $\mathcal{B}_z$. On the contrary, when the input temperature is cold ($\beta_1 \gg 1$) the machine works as a heat pump, heating up $\mathcal{B}_z$. Hence we see that the machine works as a sort of inverter for the temperature.

In order to build a NOT gate, we must add another ingredient. Indeed, the effect of the collector is basically a linear inversion; more precisely, the output inverse temperature β_z is a linear function of the input inverse temperature β_1, as we will see below. A device with such a linear response will be prone to errors, hence we must introduce some non-linearity in order to approach the typical response function of the NOT gate (inverted step function). This will be provided by the second part of the machine, namely the modulator. It is composed of an additional qubit, in contact with another thermal bath at some fixed reference (inverse) temperature β_r. The modulator qubit is also in contact with the output environment $\mathcal{B}_z$ (see Fig. 2a). This has the effect to delimit a specific range for the output temperatures β_z, making the response of the device

effectively non-linear and hence closer to an ideal NOT gate.

In the following we present in detail the models for the collector and the modulator, and then discuss the dynamics of the machine and its operation as a NOT gate. Finally, we investigate the trade-off between the gate performance (as given by the average error rate) and dissipation (as given by entropy production).

A. Collector

The collector $\mathcal{C}$ is composed of three qubits which we denote $\mathcal{C}_i$ for $i \in \{0, 1, z\}$ (see Fig. 2a), with energy gaps ϵ_i. Each qubit is weakly coupled to an environment, denoted $\mathcal{B}_i$, at (inverse) temperatures β_i with the coupling constants γ for $\mathcal{C}_0$ and $\mathcal{C}_1$ and μ for $\mathcal{C}_z$. This three-qubit system is described by a joint state $\rho_{\mathcal{C}}$ that evolves according to the master equation (3), i.e.

$$\dot{\rho}_{\mathcal{C}} = -i[H_0 + H_{\text{int}}, \rho_{\mathcal{C}}] + \mathcal{L}[\rho_{\mathcal{C}}], \tag{7}$$

with $H_0 = \sum_{i \in \{0,1,z\}} \epsilon_i |1\rangle\langle 1|_{\mathcal{C}_i}$ and $\mathcal{L} = \mathcal{L}^{(0)} + \mathcal{L}^{(1)} + \mathcal{L}^{(z)}$.

It is important that energy can flow between the qubits. For this, we choose the energy gap of the third qubit $\mathcal{C}_z$ to be $\epsilon_z = \epsilon_0 - \epsilon_1$. This implies that the two states $|1\rangle_{\mathcal{C}_0} |0\rangle_{\mathcal{C}_1} |0\rangle_{\mathcal{C}_z}$ and $|0\rangle_{\mathcal{C}_0} |1\rangle_{\mathcal{C}_1} |1\rangle_{\mathcal{C}_z}$ have the same energy. This allows us couple these two states via the interaction Hamiltonian

$$H_{\text{int}} = \chi |1\rangle\langle 0|_{\mathcal{C}_0} \otimes |0\rangle\langle 1|_{\mathcal{C}_1} \otimes |0\rangle\langle 1|_{\mathcal{C}_z} + \text{h.c.}, \tag{8}$$

where χ is the coupling strength. Importantly this interaction conserves the total energy (since $[H_0, H_{\text{int}}] = 0$) which guarantees that energy can be exchanged even in the weak coupling regime.

We are interested in the steady-state behavior of the collector, i.e. the regime where $\dot{\rho}_{\mathcal{C}} = 0$. Specifically, we would like to understand the effect of the collector on the output environment $\mathcal{B}_z$. To do so, it will be useful to follow the approach of Ref. [32]. Specifically, the idea is to describe the effect of the machine as producing a virtual qubit and putting it in thermal contact with the output environment. By characterizing the temperature of this virtual qubit, called the virtual temperature, we will capture the effect of the machine on the output environment.

First, note that from the form of the interaction Hamiltonian H_{int}, we see that there are only two states of the machine that take an active role in the steady-state dynamics. These are simply the two states that have the same energy discussed above. Now let us think of the three-qubit system as a machine part, comprising the first two qubit $\mathcal{C}_0$ and $\mathcal{C}_1$, and a target qubit $\mathcal{C}_z$. The effect of the machine part on the target is to thermalize it with a virtual qubit characterized by the following two levels:

$$|0\rangle_v := |0\rangle_{\mathcal{C}_0} |1\rangle_{\mathcal{C}_1}, \tag{9}$$

$$|1\rangle_v := |1\rangle_{\mathcal{C}_0} |0\rangle_{\mathcal{C}_1}. \tag{10}$$

Indeed these levels form an effective system with energy gap $\epsilon_v = \epsilon_0 - \epsilon_1$, a so-called virtual qubit (see also [60]). Let us denote with $g_v := \langle 1|_v \tau_{\mathcal{C}_0}(\beta_0) \otimes \tau_{\mathcal{C}_1}(\beta_1) |1\rangle_v$ the occupation of the excited state of this effective system. Then, the ratio of populations in the subspace associated with the virtual qubit becomes $g_v/(1 - g_v) = e^{-\beta_v(\epsilon_0 - \epsilon_1)}$, where β_v is the (inverse) virtual temperature:

$$\beta_v = \left(\frac{\epsilon_0}{\epsilon_0 - \epsilon_1} \right) \beta_0 - \left(\frac{\epsilon_1}{\epsilon_0 - \epsilon_1} \right) \beta_1. \tag{11}$$

Notice that the virtual temperature can be negative, which corresponds to a population inversion in the virtual qubit [32]. With this, we are now in position to understand the steady-state dynamics of the collector $\mathcal{C}$. Effectively, the collector aims to thermalize the target qubit $\mathcal{C}_z$ to the virtual temperature β_v. This can be seen by rewriting the interaction Hamiltonian in Eq. (8) in terms of the virtual qubit levels: $H_{\text{int}} = \chi(|1\rangle\langle 0|_v \otimes |0\rangle\langle 1|_{\mathcal{C}_z} + \text{h.c.})$. When $\beta_v > \beta_z$ energy flows from the machine part (via the virtual qubit) to the target qubit $\mathcal{C}_z$, effectively cooling it down; the machine acts as a refrigerator. On the other hand, when $\beta_v < \beta_z$, energy flows towards the qubit $\mathcal{C}_z$, heating it up in the process; the machine acts as a heat pump. Importantly, which one of these different machine's behaviors actually occurs depends on the inverse temperatures β_0 and β_1 via Eq. (11). This is the basic principle behind our inverter, as well as for the general model of a thermodynamic neuron, as we will see in the next section.

In turn, this will have the effect to thermalize the output environment $\mathcal{B}_z$ to the virtual temperature. To see this, let us consider the steady-state current from the collector $\mathcal{C}$ to the output environment $\mathcal{B}_z$:

$$j_{\mathcal{C}} := \mu \epsilon_z \left[g_z(\beta_z) - g_z(\beta_v) \right], \tag{12}$$

where $g_z(x) := g(x\epsilon_z)$ and g is the Fermi-Dirac distribution from Eq. (2). Indeed, the collector attempts to bring the temperature β_z of the environment $\mathcal{B}_z$ closer to the virtual temperature β_v.

By choosing energy gaps ϵ_0 and ϵ_1 appropriately [i.e. the linear weights in Eq. (11)], we can in principle obtain an inverting behaviour. However, an inverter with such a linear characteristics would be highly sensitive to errors in the input signal. In order to improve its robustness to noise we must modulate the machine's response in a way that decreases the probability of giving the wrong output. This is the main role of the modulator.

B. Modulator

The modulator $\mathcal{M}$ is composed of a single qubit with an energy gap $\epsilon_{\mathcal{M}} = \epsilon_z$. This system is put in contact with a thermal bath $\mathcal{B}_r$ at inverse temperature β_r, with coupling rate γ. The modulator qubit is also placed in contact with the finite output reservoir $\mathcal{B}_z$, with a coupling rate μ'. The qubit state $\rho_{\mathcal{M}}$ evolves according to the following master equation:

$$\dot{\rho}_{\mathcal{M}} = \mathcal{L}^{(r)}[\rho_{\mathcal{M}}] + \mathcal{L}^{(z)}[\rho_{\mathcal{M}}]. \tag{13}$$

In the steady-state the excited-state population of the qubit depends only on the rates γ and μ'. We will set the rates so
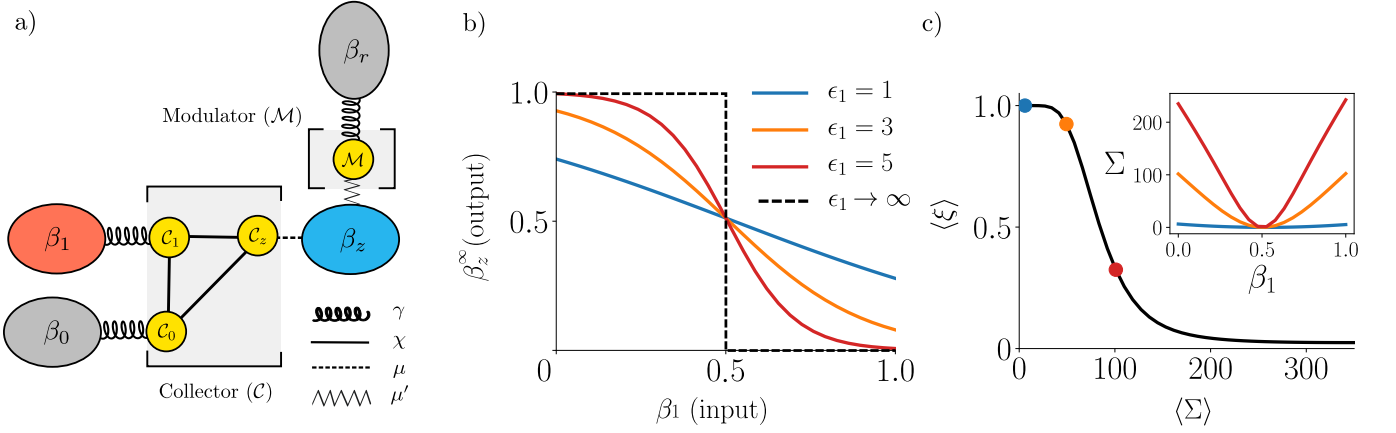
FIG. 2. **Thermodynamic neuron for implementing a NOT gate.** Panel (a) shows the design of the machine. The collector consists of three interacting qubits (yellow dots), each connected to a thermal environment. The logical input is encoded in the temperature β_1 of the heat bath $\mathcal{B}_1$ (red) while the output will be retrieved from the final temperature β_z of the finite-size reservoir $\mathcal{B}_z$ (blue); the heat bath $\mathcal{B}_0$ is at fixed reference temperature. The collector implements the desired inversion of the temperature. To make the response non-linear, we must add the modulator, which consists of an additional qubit connected to a reference heat bath. Panel (b) shows the relation between the input temperature β_1 and the final output temperature β_z^∞ (in the steady-state regime). Notably, the machine produces the desired inversion of the temperature. The quality of the response can be increased by tuning the machine parameters, in particular by increasing the energy gap ϵ_1 of the collector qubit $\mathcal{C}_1$. In the limit $\epsilon_1 \to \infty$ we obtain an ideal NOT gate (dashed black line). Panel (c) shows the trade-off between the average dissipation $\langle \Sigma \rangle$ [see Eq. (24)] and the average error $\langle \xi \rangle$ [see Eq. (22)]. We see clearly that in order to increase robustness to noise, the machine must dissipate more heat to the environment. The inset shows the entropy production as a function of the input temperature β_1 for different values of the qubit energy ϵ_1. Parameter values: $\beta_{\text{hot}} = 0$, $\beta_{\text{cold}} = 1$, $\gamma = \chi = 1$, $\mu = 10^{-4}$, $\epsilon_z = 0.1$, $\tau = 10^8$ and $\beta_0 = \beta_z(0) = 1/2$.

that $\mu' \ll \gamma$, ensuring that the qubit will effectively thermalize to the inverse temperature β_r. Therefore, the steady-state heat current from $\mathcal{M}$ to $\mathcal{B}_z$ is given by

$$j_{\mathcal{M}} := \mu' \epsilon_z \left[g_z(\beta_z) - g_z(\beta_r) \right]. \qquad (14)$$

With this we can understand the effect of the modulator on the output environment $\mathcal{B}_z$. The modulator attempts to bring β_z closer to the (inverse) temperature β_r and the strength of this effects is controlled by the coupling rate μ'. The choice of the values of β_r and μ' will specify the behavior of the modulator. By appropriately choosing these two parameters, we can tune the range of the output temperature β_z, which will generate the desired non-linearity in the response of the machine (see Appendix A).

C. Dynamics of the machine

We will now combine our understanding of the collector and the modulator to gain insight into the full evolution of the machine. The collector and the modulator are both connected to an environment $\mathcal{B}_z$ with a finite heat capacity C. The temperature change of this environment is proportional to the sum of all entering heat currents. Specifically, we assume that β_z changes according to the calorimetric equation

$$\dot{\beta}_z = \frac{1}{C}(j_C + j_{\mathcal{M}}). \qquad (15)$$

Crucially, the couplings of the collector and the modulator to $\mathcal{B}_z$ are set to be much weaker than their couplings to the heat

baths $\mathcal{B}_0$, $\mathcal{B}_1$ and $\mathcal{B}_r$, i.e. we have that $\gamma \gg \mu, \mu'$. This implies that the dynamics of the whole machine has two intrinsic time scales. The first (fast dynamics) is associated with the internal evolution of $\mathcal{C}$ and $\mathcal{M}$. Hence, both the collector and the modulator will reach their steady-states relatively quickly. This means that the qubit $\mathcal{C}_z$ of the collector will reach the virtual temperature β_v [see Eq. (11)], while the modulator qubit will be at temperature β_r. The second (slow dynamics) is associated with the changes of the temperature of the output environment $\mathcal{B}_z$. This means that $\mathcal{B}_z$ will slowly thermalize via the contact with qubits $\mathcal{C}_z$ and $\mathcal{M}$, to an intermediate temperature between β_v and β_r.

Let us now discuss the slow evolution more carefully. We denote by $\beta_z(t)$ the time evolution of the temperature of the output environment $\mathcal{B}_z$. The heat currents delivered from both parts of the machine alter $\beta_z(t)$ according to Eq. (15). The steady-state of the output environment $\mathcal{B}_z$ is achieved when $\dot{\beta}_z(t) = 0$. Denoting the stationary value of $\beta_z(t)$ with β_z^∞ we obtain an expression for its excited state population

$$g_z(\beta_z^\infty) = \Delta g_z(\beta_v) + (1 - \Delta)g_z(\beta_r), \qquad (16)$$

where $\Delta := \mu/(\mu' + \mu)$. In order to interpret the temperature of the output reservoir $\mathcal{B}_z$ as a valid logical signal we need to delimit a clear range of temperatures (see next subsection): from β_{cold} to β_{hot}. This can be done by fixing the parameters of the modulator (see Appendix A). Choosing μ' and β_r so that $\Delta = g_z(\beta_{\text{hot}}) - g_z(\beta_{\text{cold}})$ and $g_z(\beta_r) = g_z(\beta_{\text{cold}})/(1 - \Delta)$, leads to

$$\beta_z^\infty = \frac{1}{\epsilon_z} \log \left[Q(\beta_v)^{-1} - 1 \right], \qquad (17)$$

with $Q(\beta_v) := g_z(\beta_{\text{hot}})g_z(\beta_v) + g_z(\beta_{\text{cold}})(1 - g_z(\beta_v))$ and β_v is the virtual temperature given in Eq. (11).

At this point, we are ready to discuss the performance of our inverter. In Fig. 2b we plot the transfer characteristics (TC) of our machine in the steady-state regime. Specifically, we see that the behaviour between the input and the output temperatures, respectively β_1 and β_z, is indeed an inversion. For a cold (hot) input temperature, the output temperature is hot (cold). Note that in the figure, we have set $\beta_{\text{cold}} = 1$ and $\beta_{\text{hot}} = 0$. More generally, from Eq. (17), we see that: (i) when $\beta_1 \to 0$ we have $\beta_z^\infty \to \beta_{\text{cold}}$, and (ii) when $\beta_1 \to \infty$ we get $\beta_z^\infty \to \beta_{\text{hot}}$.

Additionally, we can see from the figure that the quality of the NOT gate depends on the model parameters, in particular on the energy gap ϵ_1 of the collector qubit $\mathcal{C}_1$. The larger ϵ_1 becomes, the closer we get to an ideal NOT gate. In fact, it can be shown that, in the limit $\epsilon_1 \to \infty$, the TC becomes the ideal inverted step function. We investigate analytically in Appendix A the properties of the TC in Eq. (17), showing its dependence on the energies of the collector qubits ϵ_0, ϵ_1 and the inverse temperature β_0 of the reference bath. More specifically, Eq. (17) describes a function which is close to a sigmoid (or Fermi-Dirac) function $f(x) = (1 + e^x)^{-1}$, i.e.

$$\beta_z^\infty = f(x) + \mathcal{O}(\epsilon_z), \qquad (18)$$

where $x := (\epsilon_1 + \epsilon_z)(\beta_0 - \beta_1)$. When ϵ_z is small (compared to ϵ_1), the roles of the free parameters become clear: β_0 characterizes the location of the step in β_z^∞ and $\epsilon_0 \approx \epsilon_1$ describes its steepness. For larger values of ϵ_z the TC still demonstrates the desired inverting behavior, however the role of the parameters ϵ_0 and β_0 becomes a bit more complicated to interpret (see Appendix A for details).

D. Logic operation

As seen above, our device produces the desired inversion relation between the input and output temperatures. The next step is to use the machine as a NOT gate, for which we must now encode the logical information appropriately in the corresponding temperatures.

In what follows the input and output signals will be described by random variables $x, y \in \{0, 1, \varnothing\}$, where $0, 1$ represent the binary logical values and $\varnothing$ denotes an invalid result that cannot be assigned. The logical input x is encoded in the inverse temperature β_1 of heat bath $\mathcal{B}_1$, while the logical output y is decoded from the final (inverse) temperature β_z^∞ of $\mathcal{B}_z$. For that we use the mapping

$$x = \begin{cases} 0, & \beta_1 = \beta_{\text{hot}}, \\ 1, & \beta_1 = \beta_{\text{cold}}, \end{cases} \quad y = \begin{cases} 0, & \beta_z^\infty \leq (1+\delta)\beta_{\text{hot}}, \\ 1, & \beta_z^\infty \geq (1-\delta)\beta_{\text{cold}}, \\ \varnothing & \text{otherwise}. \end{cases} \quad (19)$$

Parameters β_{cold} and β_{hot} characterize the machine's range of operation, while δ captures its robustness to noise in the output signal. Indeed, mapping logical values to intervals as above allows one to tolerate fluctuations in the output signal, i.e. interpret them correctly even if they differ between rounds due

to the stochasticity of the machine's evolution. In principle we could also consider having noise in the input signal, however, to keep the presentation simple, we will not do this here.

Naturally, the computational process is stochastic and the actual machine's output temperature will generally fluctuate around the steady-state value from Eq. (17). This will lead to possible errors in the gate implementation. Characterizing these errors is important to assess the quality of the gate, in terms of its robustness to noise.

In the following, we describe the machine as a binary channel defined by the encoding $e(\beta_1|x)$ and decoding $d(y|\beta_z^\infty)$ as specified in Eq. (19). The input distribution is denoted $p(x)$. The behaviour of the machine is then specified by a conditional distribution

$$p(y|x) := \int d(y|\beta_z)T(\beta_z|\beta_1)e(\beta_1|x)\, d\beta_1 d\beta_z, \qquad (20)$$

where $T(\beta_z|\beta_1)$ describes the actual response β_z of the machine to the input β_1. Since the evolution is ultimately stochastic, we assume that the response takes the form

$$T(\beta_z|\beta_1) = \frac{1}{\sqrt{2\pi}C}e^{\frac{-(\beta_z - \beta_z^\infty)^2}{2C^2}}, \qquad (21)$$

so that the machine's output follows a normal distribution around the steady-state response β_z^∞ with variance proportional to the heat capacity of the finite-size output environment.

The average computation error $\langle \xi \rangle$ is the probability of observing an output different from the desired one, i.e.

$$\langle \xi \rangle = \sum_{x \in \{0,1\}} \sum_{y \in \{0,1\}} p(x)p(y|x)\delta(x - y). \qquad (22)$$

This quantity is directly related to the shape of the transfer curve (TC), see Fig. 2b. Notably, the closer TC is to an ideal NOT gate (black dashed line), the smaller is $\langle \xi \rangle$. Interestingly, the actual TC of our machine approaches the ideal one in the limit of $\epsilon_1 \to \infty$. This indicates that the quality of the computation can be enhanced at the cost of using more energy, which implies that the machine will dissipate more heat. In the following discussion, we will examine this trade-off in more detail.

E. Trade-off between entropy production and noise robustness

Here we investigate the relation between the quality of the gate, as quantified by the average computation error, to its thermodynamic cost, given by the amount of entropy that is produced during the computation.

First, let us evaluate the entropy production. As mentioned the dynamics of the machine features two different time scales. The primary source of dissipation is given by the slow dynamics, in which the temperature of the output reservoir changes. The latter being connected to the collector and the modulator, the total dissipation rate is given by $\dot{\Sigma} = \dot{\Sigma}_\mathcal{C} + \dot{\Sigma}_\mathcal{M}$. We have that $\dot{\Sigma}_\mathcal{C} = -\beta_0 j_0 - \beta_1 j_1 - \beta_z j_\mathcal{C}$

and $\dot{\Sigma}_{\mathcal{M}} = -\beta_z j_{\mathcal{M}} - \beta_r j_r$; here $j_{0,1,r}$ denotes the current from the heat bath $\mathcal{B}_{0,1,r}$ to their respective qubit. From the perspective of the slow dynamics the entropy of the qubits in the machine does not change, i.e. $\dot{S}(\rho_{\mathcal{S}}) = 0$. Because of this, the entropy production is the weighted sum of the heat dissipated in each environment. In order to quantify the total dissipation incurred during the computation, we have to integrate the dissipation rate over time, i.e.

$$\langle \Sigma(\beta_1) \rangle = \int_0^\tau \langle \dot{\Sigma}(\beta_1) \rangle \mathrm{d}t. \tag{23}$$

where τ is the running time of the computation, indicating when the final temperature output β_z^∞ is read off.

We see that this quantity depends on β_1. Hence the dissipation will vary depending on the input. In the inset of Fig. 2c, we show this behaviour, also considering different values of the parameter ϵ_1. As expected, since the rate of dissipation is proportional to the heat currents flowing into the environments, the larger the energy of the qubits, the larger the rate of heat dissipation. Moreover, as expected, when $\beta_1 = \beta_0$, dissipation vanishes.

Next, let us estimate the dissipation averaged over different rounds of the computation, i.e. averaging over the inputs. We get the quantity

$$\langle \Sigma \rangle = \sum_{x \in \{0,1\}} \int p(x) e(\beta_1 | x) \Sigma(\beta_1) \, \mathrm{d}\beta_1. \tag{24}$$

In Fig. 2c we examine the relation between the total dissipation $\langle \Sigma \rangle$ and the average computation error $\langle \xi \rangle$. We consider a uniform input distribution $p(x) = 1/2$, and a sufficiently long computing time to ensure we are close to the steady-state regime, $\tau = 10^8$. There is a monotonous relation between the two quantities. As expected, we see that lowering the average error rate comes at the price of increasing the dissipation.

IV. THERMODYNAMIC NEURON FOR LINEARLY-SEPARABLE FUNCTIONS

In the previous section we presented an autonomous thermal machine for performing a simple computation task, namely inverting a signal. In this section, we generalize this construction for performing more complex computations. In particular, we show that any linearly-separable function (from n bits to one bit) can be implemented via such a machine, and give an effective algorithm for setting the appropriate machine parameters. This represents the general form of a thermodynamic neuron. We discuss explicitly examples for implementing the NOR gate and 3-majority.

A key step will be to establish a close connection between the thermodynamic neuron and the perceptron, the standard algorithm for modeling an artifical neuron. In particular this connection exploits the notion of the virtual qubit.

A. Model

Similarly to the machine for inversion, the general model of a thermodynamic neuron consists of two main parts, the collector $\mathcal{C}$ and the modulator $\mathcal{M}$ (see Fig. 3). The design of the collector is a generalisation of the previous one, while the modulator is exactly the same. Again, the function of the collector is to modify the temperature of the output reservoir depending on the temperature of the input baths (that encode the input of the computation). To do so, the machine will be designed as to prepare a virtual qubit, the temperature of which then encodes the output of the computation. The output reservoir is then put in contact with a collector qubit at the virtual temperature. The role of the modulator is again to set the temperature range for the output reservoir, which provides the required non-linearity for the computation.

Consider the implementation of a function from n bits to one bit. We now describe the general structure of the machine, starting with the collector. The latter now consists of $n+2$ qubits denoted as $\mathcal{C}_i$, with energy gaps ϵ_i. The first qubit $\mathcal{C}_0$ is connected to a heat bath $\mathcal{B}_0$ at fixed reference temperature β_0. The qubits $\mathcal{C}_1$ to $\mathcal{C}_n$ are connected to the input heat baths, their temperatures (β_1 to β_n) encoding the n input bits. Finally, the last qubit $\mathcal{C}_z$ is connected to the output reservoir $\mathcal{B}_z$ with a finite heat capacity C. The modulator is exactly as before. It consists of a single qubit, connected to a heat bath at a reference temperature β_r, as well as to the output reservoir $\mathcal{B}_z$.

At this point we have not yet specified the machine design. That is, we have not set the qubit energy gaps ϵ_i, and we have not specified the form of the interaction Hamiltonian. These parameters will depend on the exact form of the logical function we would like to implement. This is in general a non-trivial problem, but we will see below an algorithm for effectively setting the appropriate machine parameters.

Before doing so, it is useful to introduce again the virtual qubit, the temperature of which will again encode the desired output of the computation. The virtual qubit is a two-dimensional subspace within the $n + 1$ collector qubits $\mathcal{C}_0, ..., \mathcal{C}_n$. Specifically, it consists of the two energy levels

$$|0\rangle_v := |h_0\rangle_{\mathcal{C}_0} |h_1\rangle_{\mathcal{C}_1} \cdots |h_n\rangle_{\mathcal{C}_n}, \tag{25}$$

$$|1\rangle_v := |h_0 \oplus 1\rangle_{\mathcal{C}_0} |h_1 \oplus 1\rangle_{\mathcal{C}_1} \cdots |h_n \oplus 1\rangle_{\mathcal{C}_n}, \tag{26}$$

where $\oplus$ denotes addition mod 2. The virtual qubit is thus characterized by an interaction vector $\boldsymbol{h} = (h_0, h_1, \ldots, h_n)$. The energy gap of the virtual qubit, denoted ϵ_v, is given by

$$\epsilon_v := \sum_{i=0}^n (-1)^{h_i \oplus 1} \epsilon_i \tag{27}$$

The design of the machine is then completely characterized by the interaction vector $\boldsymbol{h}$ and the energy gaps ϵ_i for $i \in \{0, 1, \ldots, n\}$.

As in the previous section, the main idea of the machine is to engineer a virtual qubit at the desired temperature, and place it in thermal contact with the output qubit $\mathcal{C}_z$, which in turn will then thermalize the output reservoir $\mathcal{B}_z$. To do so,
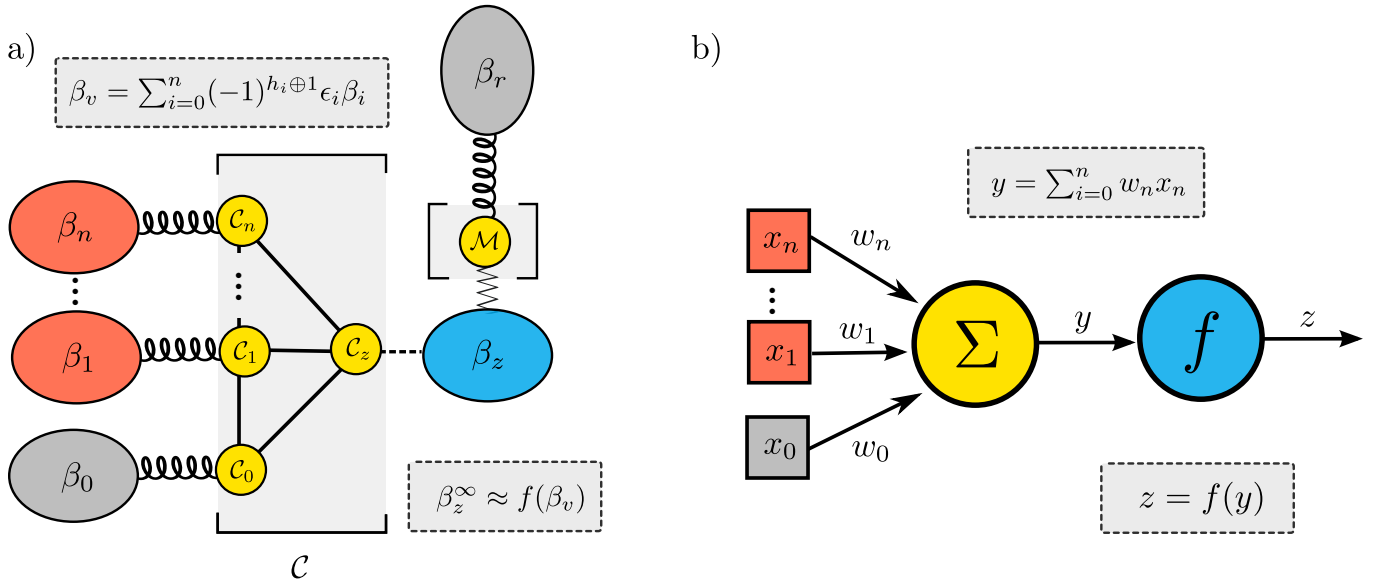
FIG. 3. **General model of the thermodynamic neuron and analogy with a perceptron.** Panel (a) shows the structure of a thermodynamic neuron for implementing an n-to-one bit function. The collector $\mathcal{C}$ consists of $n + 2$ qubits, connected to the input heat baths (red), reference heat baths (grey), as well as the output reservoir (blue). The working principle of the collector is to thermalize qubit $\mathcal{C}_z$ to the virtual temperature β_v (see Eq. (29)). In turn, this affects the temperature of the finite-size output reservoir $\mathcal{B}_z$ (blue). The modulator controls the range of output temperatures, making the response effectively non-linear. In the steady-state regime, the final output temperature is given by β_z^∞ given by a non-linear function of β_v [see Eqs (30) and (31)]. The machine can implement any linearly-separable binary function by appropriately setting the parameters: the qubit energies, the interaction Hamiltonian and the temperatures of the reference heat baths. Notably, this machine is closely connected to the perceptron model shown in panel (b), which is used extensively in machine learning. Given inputs x_k, the perceptron first computes a weighted sum y, then processed via a non-linear activation (sigmoid) function f. Similarly, the thermodynamic neuron first creates a virtual qubit at temperature β_v, which is a weighted sum of the input temperatures β_k. Second, the modulator implements the non-linear activation function. Note that in a specific regime (ϵ_z sufficiently small), the thermodynamic neuron implements a perceptron, as the activation function tends to a sigmoid in this case.

we must set qubit $\mathcal{C}_z$ to be resonant with the virtual qubit, i.e. $\epsilon_z = \epsilon_v$, and the interaction Hamiltonian to the form $H_{\text{int}} := g(|0\rangle\langle1|_v \otimes |1\rangle\langle0|_{\mathcal{C}_z} + \text{h.c.})$.

To understand the action of the machine, let us now characterize the temperature of the virtual qubit. The excited-state population of the virtual qubit in the steady-state becomes

$$g_v(\beta_v) := g_0(h_0) \cdot g_1(h_1) \cdot \ldots \cdot g_n(h_n), \qquad (28)$$

where $g_i(0) = (1 + e^{-\beta_i \epsilon_i})^{-1}$ and $g_i(1) = 1 - g_i(0)$. The virtual temperature β_v satisfies $\exp[-\beta_v \epsilon_v] = g_v(\beta_v)/(1 - g_v(\beta_v))$, and is given by (see Appendix B)

$$\beta_v = \frac{1}{\epsilon_z} \sum_{i=0}^{n} (-1)^{h_i} \beta_i \epsilon_i. \qquad (29)$$

Importantly, we see that the virtual temperature is given by a linear combination of the input temperatures β_i, with relative weights given by the energy gaps ϵ_i. This relation will be crucial in the next subsection where we establish a connection with perceptrons.

We can now discuss the dynamics of the machine, which is governed by a master equation of the form (3) with $H_0 := \sum_{i=0}^{n} \epsilon_i |1\rangle\langle1|_{\mathcal{C}_i} + \epsilon_z |1\rangle\langle1|_{\mathcal{C}_z}$ and H_{int} specified above. The dissipator is given by: $\mathcal{L}[\cdot] = \sum_{i=0}^{n} \mathcal{L}^{(i)}[\cdot] + \mathcal{L}^{(z)}[\cdot]$, where each dissipator $\mathcal{L}^{(k)}$ takes the form of Eq. (4). Similarly to

the machine for inversion, the device will feature two natural time-scales: thermalization within the collector and modulator will happen quickly, while the coupling to the output environment $\mathcal{B}_z$ is much weaker. The time evolution of the output temperature $\beta_z(t)$ will thus be governed by the slow dynamics and given by Eq. (15).

Similarly as before, we can solve for the inverse temperature β_z^∞ in the steady-state regime [see Eq. (16)]. More specifically, we find

$$\beta_z^\infty = \frac{1}{\epsilon_z} \log \left[Q(\beta_v)^{-1} - 1 \right], \qquad (30)$$

with $Q(\beta_v) := g_z(\beta_{\text{hot}}) g_z(\beta_v) + g_z(\beta_{\text{cold}})(1 - g_z(\beta_v))$ and β_v is given by Eq. (29). Note that, as before, the temperatures β_{cold} and β_{hot} define the desired temperature range for the computation. Following the derivation in the previous section, we can expand β_z^∞ in the energy gap ϵ_z and obtain

$$\beta_z^\infty = f(\beta_v) + O(\epsilon_z), \qquad (31)$$

where $f(x) = (1 + e^x)^{-1}$. Therefore, we see that for small ϵ_z, the output temperature β_z^∞ behaves essentially as the sigmoid function. For larger values of ϵ_z the function differs from the sigmoid one, but still offers a similar qualitative behavior.

B. Connection with perceptrons

At this point, it is insightful to establish a formal connection between our model of the thermodynamic neuron and the perceptron [61]. The latter represents the most common model of an artificial neuron, and serves as a fundamental component of artificial neural networks.

The perceptron (see Fig. 3b) is a simple algorithm for linear binary classification [62]. For a vector of inputs $\boldsymbol{x} = (x_0, \ldots, x_n)$ it produces an output z given by

$$z = f(y) \qquad \text{with} \quad y = \sum_{i=0}^{n} x_i w_i, \qquad (32)$$

where $x_0 = 1$ by convention, $\boldsymbol{w} = (w_0, \ldots, w_n)$ is a vector of weights that specifies the behavior of the perceptron, and f is the activation function (sigmoid). The perceptron allows for a classification of the input space into two classes; it provides a linear separation of the the inputs depending on the value of the function (0 or 1).

At this point, the connection appears clearly. The thermodynamic neuron computes via a two-step procedure, that is very similar to the perceptron. First, given the inputs (encoded here in the temperatures β_k), the collector produces a virtual qubit, whose virtual temperature is given by a weighted sum of the input temperatures, with weights given by the energies ϵ_k; see Eq. (29). This corresponds exactly to the computation of the weighted sum y in the perceptron. Second, through the effect of the modulator, the output response becomes non-linear, and the final temperature β_z^∞ is given by a nonlinear function of the virtual temperature, see Eq. (30). In particular, in the regime of small ϵ_z, this nonlinear functions becomes the sigmoid activation function f, hence corresponding exactly to the case of the perceptron, see Eq. (31). This analogy is important, and is further illustrated on Fig. 3.

An interesting insight from this analogy is that it sheds light on the importance of the modulator in our model. Indeed, if the machine would involve only the collector, the final output temperature would be simply the virtual temperature, corresponding to a trivial activation function $f(y) = y$ in the perceptron algorithm, which is known to perform poorly in machine learning.

Hence the modulator provides the essential ingredient of non-linearity. Its effect is to map the the virtual temperature in a non-linear way within the temperature range from β_{cold} to β_{hot}. More specifically, the (final) output steady-state temperature β_z^∞ becomes a non-linear function of β_v, as in Eq. (30). Depending on the value of ϵ_z we get different types of non-linear function. In particular, when ϵ_z is small, we get the sigmoid function as in a perceptron. This suggests that thermodynamic neurons could serve as a physical model for a fully analogue implementation of perceptrons.

C. Algorithm for designing the machine

Beyond the conceptual interest, the above connection between the perceptron and our thermodynamic neuron is use-ful. Notably, this provides a general method for designing a thermodynamic neuron for performing a desired logic operation. We will see that any function that is linearly separable can be implemented.

Specifically, suppose we want to implement an n-input binary function $R(\boldsymbol{x})$, where $\boldsymbol{x} = (x_1, \ldots, x_n)$. First, we define the mapping between logical inputs and outputs and temperatures. The logical inputs and output are denoted with $x_1, \ldots x_n, y \in \{0, 1\}$, and encoded in the inverse temperatures of the respective environments through the following procedure:

$$x_i = \begin{cases} 0, & \beta_i = \beta_{\text{hot}}, \\ 1, & \beta_i = \beta_{\text{cold}}, \end{cases} \quad y = \begin{cases} 0, & \beta_z^\infty \le (1+\delta)\beta_{\text{hot}}, \\ 1, & \beta_z^\infty \ge (1-\delta)\beta_{\text{cold}}, \\ \varnothing & \text{otherwise.} \end{cases} \quad (33)$$

where $i \in \{1, \ldots, n\}$. As before, we focus on the range of temperatures from β_{cold} and β_{hot}.

Next we construct a thermodynamic neuron implementing $R(\boldsymbol{x})$. For this, we must appropriately set the parameters of the machine, namely β_0, ϵ_k for $k \in \{0, 1, \ldots, n\}$ and the interaction Hamiltonian. For that we can use the following algorithm.

Algorithm 1: Designing the thermodynamic neuron

Input: n, $R(\boldsymbol{x})$, ϵ_z, α
Output: β_0, ϵ_k and h_k for $k \in \{0, 1, \ldots, n\}$

Proceed according to the following steps:

1. Construct a training set $D := \{(\boldsymbol{x}^{(i)}, y_i)\}_{i=1}^{2^n}$, where $\boldsymbol{x}^{(i)} = (x_1^{(i)}, \ldots, x_n^{(i)})$ and $y_i = R(\boldsymbol{x}^{(i)})$.

2. Train a linear classifier (e.g. a sigmoid perceptron) to classify $\boldsymbol{x}_i$ into two classes: $y_i = 0$ and $y_i = 1$. This gives a vector of weights $\boldsymbol{w} = (w_0, \ldots, w_n)$.

3. Set the elements of the vector $\boldsymbol{h} = (h_0, \ldots, h_n)$ as

$$h_k = \begin{cases} 0 & \text{if} \quad w_k \ge 0, \\ 1 & \text{if} \quad w_k < 0. \end{cases} \qquad (34)$$

4. Set qubit energies ϵ_k as

$$\epsilon_k = \begin{cases} \alpha|\epsilon_z - \sum_{k=1}^{n} w_k| & \text{if} \quad k = 0, \\ \alpha|w_k| & \text{otherwise.} \end{cases} \qquad (35)$$

5. Set the bias inverse temperature β_0 as

$$\beta_0 = \frac{|w_0|}{|\epsilon_z - \sum_{k=1}^{n} w_k|}. \qquad (36)$$

To see why the above algorithm works, let us observe that

the virtual temperature from Eq. (29) becomes

$$\beta_v = \frac{1}{\epsilon_z}\left[(-1)^{i_0}\beta_0\epsilon_0 + \sum_{k=1}^{n}(-1)^{i_k}\beta_k\epsilon_k\right] \tag{37}$$

$$= \frac{\alpha}{\epsilon_z}\left[w_0 + \sum_{k=1}^{n}w_k\beta_k\right]. \tag{38}$$

Using the expansion from Eq. (31) we have

$$\beta_z^{\infty} = f(x) + \mathcal{O}(\epsilon_z), \quad x = \alpha\left(w_0 + \sum_{i=1}^{n}w_k\beta_k\right), \tag{39}$$

which is exactly the output of the perceptron algorithm for a sigmoid activation function. Eq. (39) also reveals the role of parameter α which quantifies the steepness of the threshold separating the two outputs, or in other words, the quality of implementing the desired function. In general, α acts as a rescaling of all the energies ϵ_k for $k = 0, ..., n$ of the qubits of the collector. Hence, increasing α leads to more dissipation and also lowers the errors in the computation. In particular, for the NOT gate, one can see that $\alpha = \epsilon_1$.

To illustrate how to design a thermodynamic neuron using Algorithm 1 we now provide two examples.

D. Example 1: NOR gate

The NOR gate takes $n = 2$ input bits and returns as output the negative OR (see truth table Fig. 4a). To design the thermodynamic neuron we follow the steps discussed in Algorithm 1. Using the truth table of NOR, we first construct the set D of $2^n = 4$ data points (see Fig. 4b). In principle, we could now run the algorithm and determine the vector of weights w. Since in this case the separating hyperplane can be found by hand, we simply choose $x_1 + x_2 = 1/2$. This leads to the vector of weights $w = (1, -2, -2)$. Consequently, the interaction vector h and energy vector $\epsilon := (\epsilon_0, \epsilon_1, \ldots, \epsilon_n)$ become

$$h = (0, 1, 1), \qquad \epsilon = \alpha(\epsilon_z + 4, 2, 2), \tag{40}$$

with the reference (inverse) temperature $\beta_0 = (\epsilon_z + 4)^{-1}$. This choice of parameters leads to the virtual temperature

$$\beta_v = \alpha(1 - 2\beta_1 - 2\beta_2). \tag{41}$$

The machine's response β_z^{∞} is then given by Eq. (29) with β_v as given above. In Fig. 4c we plot the response of the thermodynamic neuron as a function of the input temperatures β_1 and β_2. The pattern of output temperatures clearly matches the desired NOR function.

Notably, the NOR function is functionally complete, i.e. any logic function on any number of inputs can be constructed using only NOR functions as building blocks. Consequently, by connecting multiple thermodynamic neurons appropriately one can in principle carry out any classical computation. This shows that the thermodynamic neuron is a universal.
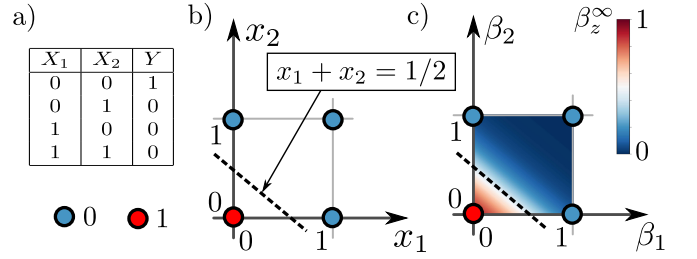

FIG. 4. **Example 1: NOR.** Analysis of the thermodynamic neuron for implementing the NOR function. The truth table of NOR is given in panel (a). Panel (b) shows all possible logical states of the machine (blue and red dots) where the colour corresponds to the desired output. Panel (c) shows the response β_z^{∞} of the thermodynamic neuron as a function of the inputs β_1 and β_2. The device does indeed implement the desired NOR gate.
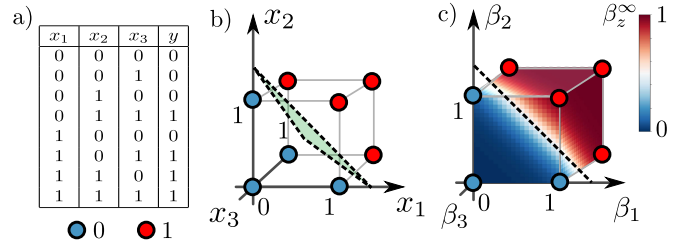

FIG. 5. **Example 2: 3-majority.** Analysis of the thermodynamic neuron for implementing the majority function on three input bits. Panel (a) shows the truth table. Panel (b) shows the possible logical states of the machine. The separating hyperplane (dashed line) is specified by the equation $x_1 + x_2 + x_3 = 4/3$. Panel (c) shows the machine's response β_z^{∞} as a function of the inputs β_1, β_2 and β_3. We see that the machine implements the desired operation.

E. Example 2: 3-majority

The 3-majority function takes $n = 3$ inputs bits and outputs the majority. Its truth table is shown in Fig. 5a. To implement 3-majority using a thermodynamic neuron we again use Algorithm 1. We construct the training set D of $2^n = 8$ data points (see Fig. 5b). Using the algorithm we found a vector of weights $w = (-4, 3, 3, 3)$. The interaction vector h and the energy vector ϵ are then given by

$$h = (1, 0, 0, 0), \qquad \epsilon = \alpha(\epsilon_z + 12, 3, 3, 3), \tag{42}$$

and the reference temperature is given by $\beta_0 = (\epsilon_z + 12)^{-1}$. This choice of parameters leads to the virtual temperature

$$\beta_v = \alpha(4 - 3\beta_1 - 3\beta_2 - 3\beta_3). \tag{43}$$

As before, the machine's response β_z^{∞} is given by Eq. (29) with β_v specified above. In Fig. 5c we plot the response of the thermodynamic neuron as a function of the input temperatures β_1, β_2 and β_3. The pattern of the output temperatures matches the desired 3-majority function.

F. Limitations

From the close connection with perceptrons, we can immediately deduce a general limitation on the class of functions that can be implemented via a single thermodynamic neuron, namely linearly separable functions.

In fact, it is known that perceptron can only represent functions that are linearly separable [63]. These are functions for which the set of inputs for which the function takes value 0 can be separated from those whose output is 1 via a simple hyperplane. Consequently, this constraint also limits the range of functions that can be modeled using a single thermodynamic neuron. It is however possible to overcome this limitation by considering networks of neurons. In the next section we will how networks of thermodynamic neurons can be used to compute any binary function.

V. NETWORK OF THERMODYNAMIC NEURONS

Perceptrons can be assembled into a network. By increasing the complexity of such a network, the model gains the ability represent more complex functions. According to the universal approximation theorem, a network with sufficiently many layers of perceptrons can approximate any function [64]. From the close connection discussed in the previous section, this shows that thermodynamic neurons, when combined in a network, can in principle implement any function.

In practice, however, determining the design of a network of thermodynamic neurons for implementing a specific function is non-trivial. Again, we can take inspiration from artificial neural networks, and we can use an extension of Algorithm 1. More specifically, suppose we want to implement an n-input binary function $R(\boldsymbol{x})$. To construct the network for implementing $R(\boldsymbol{x})$ we must first choose the structure of the network, i.e. the number of layers, the number of thermodynamic neurons in each layer and the connectivity. Next we have to appropriately tune the parameters of each of thermodynamic neuron, namely its reference temperature β_0, the energy gaps ϵ_k and the interaction Hamiltonian. These parameters can be determined using Algorithm 1 with the difference that now the training step (Step 2) should be performed on the whole network rather than a single thermodynamic neuron. To illustrate this procedure, we present below a network with three thermodynamic neurons for implementing the XOR function, which is not linearly separable.

Before proceeding to the example, we comment on an interesting aspect of these networks. They will typically involve feeding the output of certain neurons into the input of another. For the above construction to work properly, we must ensure that layers are synchronized, operating one after the other. This requires a timing device for coupling the neurons in the appropriate way. In fact, this can also be done autonomously, by using an autonomous clock powered by heat baths at different temperatures [45]. In parallel, it would also be interesting to see if this timing operation could be dispensed with. In this case, one would consider a network where all the thermodynamic neurons are coupled together from the start. The main
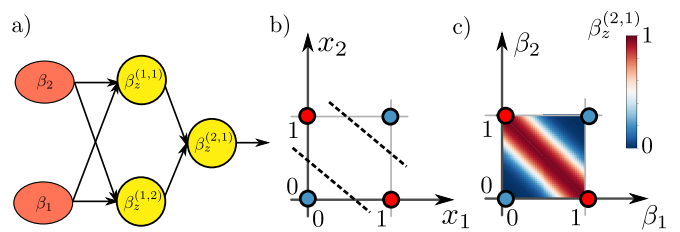

FIG. 6. **Example 3: XOR.** Panel (a) shows the structure of a network of thermodynamic neurons that can implement the XOR function. In this case the training set cannot be separated by a hyperplane (see Panel (b)), as the function is not linearly separable. The machine produces the desired response as shown in panel (c): the response β_z^∞ as a function of the inputs β_1 and β_2. Note that this machine for implementing XOR can be seen as the composition of a NAND gate and an OR gate, whose outputs $\beta_z^{(1,1)}$ and $\beta_z^{(1,2)}$ are then supplied as an input to an AND gate with output $\beta_z^{(2,1)}$.

problem in this configuration, is that one could in principle have additional (unwanted) heat currents in the device (e.g. flowing backwards), so that we can no longer guarantee the validity of Eq. (30) for thermodynamic neurons in the internal layers.

A. Example 3: XOR gate

The binary XOR function takes $n = 2$ input bits and returns the parity. It is not a linearly separable function (see Fig. 6b). Hence, it cannot be implemented with a single thermodynamic neuron. To implement XOR, we choose the network structure presented in Fig. 6a. Then, using Algorithm 1, we compute the parameters of each the thermodynamic neuron. Specifically, using the truth table of XOR, we construct the training set D of $2^n = 4$ data points (see Fig. 6b). Then we perform Step 2 of the algorithm using the standard back-propagation algorithm [65] combined with the ADAM optimization [66], obtaining the vectors of weights. Consequently, we compute the energy and the interaction vectors, as well as the reference bath temperature for each neuron. The response of the machine, i.e. the inverse temperature of the last thermodynamic neuron, is shown in Fig. 6c as a function of the input temperatures β_1 and β_2. We see that the network implements indeed the desired XOR function.

VI. DISCUSSION

In this work we introduced autonomous quantum thermal machines called *thermodynamic neurons* for performing classical computation. The machine is composed of several qubits which are coupled to thermal environments at different temperatures. The logical inputs and outputs of the computation are encoded in the temperatures of these environments. By engineering the energies and interactions of the machine's qubits, the device can implement any linearly-separable function. In particular, we discussed the implementation of NOT,

3-majority and NOR gates, the latter enabling universal computation. For more complex functions, we give an efficient algorithm for tuning the machine parameters. In turn, this algorithm can also be used for networks of thermodynamic neurons, which enable the direct implementation of any desired logical function.

A notable aspect of our machines is that they rely solely on changes in temperature and energy flows: they compute with heat. In contrast to standard (nano-scale) electronic computing devices, thermodynamic neurons are not based on building blocks such as transistors; instead they can directly implement a desired logic gate. This also differentiates our model from other alternative models of computation, notably the phonon-based computation [67–71], spintronics [72–74] or superconducting circuits [75].

Our work also brings progress from the perspective of autonomous quantum thermal machines, by demonstrating a new application for them, namely classical computation. A single thermodynamic neuron can indeed be considered an autonomous device (see [49]), while networks of them can be made autonomous via the addition of a thermodynamic clock [45]. An interesting question is whether the clock could be directly imbedded in the network of thermodynamic neurons. In parallel, our work also further demonstrates the relevance of virtual qubits and virtual temperatures [32]. This complements recent work where these notions are used for characterizing thermodynamic properties of quantum systems [76, 77], the performance of thermal machines [78, 79] and fundamental limits on thermodynamic processes [80].

Another relevant aspect is that our model is thermodynamically consistent, in the sense of complying to the laws of thermodynamics. This allowed us to investigate its thermodynamic behavior and contrast it with the machine's performance as a computing device. Specifically, for the NOT gate, we observe a clear trade-off between dissipation and performance, in terms of noise robustness. That is, enhancing the performance of the gate requires increasing dissipation. More generally, a similar trade-off relation between dissipation and performance exists for a general computation process carried out by the thermodynamic neuron. It would be interesting to pursue this direction further, e.g. prove a universal relationship by taking inspiration from thermodynamic uncertainty relations [81].

VII. OUTLOOK

Our work also opens interesting questions from the point of view of machine learning and more generally for thermodynamic computing.

As we discussed, thermodynamic neurons have a direct connection to perceptrons and neural networks. In partic-

ular, a physical implementation of thermodynamic neurons (and more generally networks of them) would provide an alternative physics-based approach for realising neural networks. This would represent a direct (analogue) implementation, hence possibly bypassing some of the challenges of more standard digital (transistor-based) simulations of neural networks. Notably, the energy requirements and heat dissipation of the latter is very significant, and looking for analogue implementations for reducing this thermodynamic cost is important, see e.g. [82]. Investigating the relevance of the thermodynamic neurons in this context is an interesting question.

From a more fundamental perspective, our model could also be used to investigate the thermodynamics of learning. One would need to devise a mechanism for autonomously changing the qubit energies based on the outcome of the computation. In this way the machine would be able to "learn" a desired behavior in a fully autonomous manner, i.e. to improve its own decisions based on reward or penalty. We believe this provides an interesting approach for modelling the process of learning in a thermodynamically consistent manner.

Our work can also be discussed from the perspective of thermodynamic computation [24, 25, 30]. Here, we believe that an interesting aspect of our model is the fact that computations are implemented in a physical process that is far out of equilibrium. Indeed, we use machines connected to multiple environments at different temperatures, and consider non-equilibrium steady-states. What computational power can we obtain from such a model? While we have seen that it can perform universal classical computation and is also naturally connected to neural networks, a key question is to determine its efficiency (notably in terms of time) for solving relevant classes of problems. For example, could this model provide a speed-up compared to classical computers for a relevant class of problems?

These are rather long-term perspectives, and a more pressing one is the potential implementation of thermodynamic neurons. In this respect, recent progress on realizing autonomous quantum thermal machines with trapped ions [50] and superconducting qubits [51], together with theoretical proposals in quantum dots [83] and cavity QED [40] are relevant. An interesting alternative is to investigate whether the physics of our model can be reproduced by a fully classical model based on rate equations. This would open the door to a classical implementation within stochatstic thermodynamics [84].

[1] C. H. Bennett, International Journal of Theoretical Physics **21**, 905 (1982).

[2] J. M. Parrondo, J. M. Horowitz, and T. Sagawa, Nature physics **11**, 131 (2015).

[3] D. H. Wolpert, Journal of Physics A: Mathematical and Theoretical **52**, 193001 (2019).

[4] R. Landauer, IBM journal of research and development **5**, 183 (1961).

[5] C. H. Bennett, IBM journal of Research and Development **17**, 525 (1973).

[6] E. Fredkin and T. Toffoli, International Journal of theoretical physics **21**, 219 (1982).

[7] D. Aharonov, M. Ben-Or, R. Impagliazzo, and N. Nisan, Limitations of noisy reversible computation (1996), arXiv:quant-ph/9611028 [quant-ph].

[8] S. Deffner and C. Jarzynski, Phys. Rev. X **3**, 041003 (2013).

[9] A. B. Boyd, D. Mandal, and J. P. Crutchfield, Phys. Rev. X **8**, 031036 (2018).

[10] P. Faist and R. Renner, Phys. Rev. X **8**, 021011 (2018).

[11] J. Gu and P. Gaspard, Physical Review E **99**, 012137 (2019).

[12] J. Gu and P. Gaspard, Phys. Rev. E **99**, 012137 (2019).

[13] D. H. Wolpert and A. Kolchinsky, New Journal of Physics **22**, 063047 (2020).

[14] C. Y. Gao and D. T. Limmer, Phys. Rev. Res. **3**, 033169 (2021).

[15] N. Freitas, J.-C. Delvenne, and M. Esposito, Physical Review X **11**, 10.1103/physrevx.11.031064 (2021).

[16] P. Helms and D. T. Limmer, arXiv preprint arXiv:2211.00670 (2022).

[17] J. Kuang, X. Ge, Y. Yang, and L. Tian, IEEE Transactions on Circuits and Systems II: Express Briefs **69**, 3729 (2022).

[18] U. Seifert, Reports on progress in physics **75**, 126001 (2012).

[19] A. Solfanelli, A. Santini, and M. Campisi, AVS Quantum Science **4**, 10.1116/5.0091121 (2022).

[20] M. Fellous-Asiani, J. H. Chai, R. S. Whitney, A. Auffèves, and H. K. Ng, PRX Quantum **2**, 040335 (2021).

[21] M. Fellous-Asiani, J. H. Chai, Y. Thonnart, H. K. Ng, R. S. Whitney, and A. Auffèves, Optimizing resource efficiencies for scalable full-stack quantum computers (2022), arXiv:2209.05469 [quant-ph].

[22] A. Auffèves, PRX Quantum **3**, 10.1103/prxquantum.3.020101 (2022).

[23] J. Stevens, D. Szombati, M. Maffei, C. Elouard, R. Assouly, N. Cottet, R. Dassonneville, Q. Ficheux, S. Zeppetzauer, A. Bienfait, A. Jordan, A. Auffèves, and B. Huard, Physical Review Letters **129**, 10.1103/physrevlett.129.110601 (2022).

[24] T. Conte, E. DeBenedictis, N. Ganesh, T. Hylton, J. P. Strachan, R. S. Williams, A. Alemi, L. Altenberg, G. Crooks, J. Crutchfield, L. del Rio, J. Deutsch, M. DeWeese, K. Douglas, M. Esposito, M. Frank, R. Fry, P. Harsha, M. Hill, C. Kello, J. Krichmar, S. Kumar, S.-C. Liu, S. Lloyd, M. Marsili, I. Nemenman, A. Nugent, N. Packard, D. Randall, P. Sadowski, N. Santhanam, R. Shaw, A. Stieg, E. Stopnitzky, C. Teuscher, C. Watkins, D. Wolpert, J. Yang, and Y. Yufik, Thermodynamic computing (2019).

[25] P. J. Coles, C. Szczepanski, D. Melanson, K. Donatella, A. J. Martinez, and F. Sbahi, Thermodynamic ai and the fluctuation frontier (2023), arXiv:2302.06584 [cs.ET].

[26] S. Goldt and U. Seifert, Phys. Rev. Lett. **118**, 010601 (2017).

[27] T. Hylton, Entropy **22**, 10.3390/e22030256 (2020).

[28] T. Hylton, Entropy **24**, 10.3390/e24060744 (2022).

[29] A. B. Boyd, J. P. Crutchfield, and M. Gu, New Journal of Physics **24**, 083040 (2022).

[30] M. Aifer, K. Donatella, M. H. Gordon, T. Ahle, D. Simpson, G. E. Crooks, and P. J. Coles, Thermodynamic linear algebra (2023), arXiv:2308.05660 [cond-mat.stat-mech].

[31] N. Linden, S. Popescu, and P. Skrzypczyk, Physical Review Letters **105**, 10.1103/physrevlett.105.130401 (2010).

[32] N. Brunner, N. Linden, S. Popescu, and P. Skrzypczyk, Physical

[33] J. Goold, M. Huber, A. Riera, L. del Rio, and P. Skrzypczyk, J. Phys. A **49**, 143001 (2016).

[34] S. Vinjanampathy and J. Anders, Contemp. Phys. **57**, 545–579 (2016).

[35] M. T. Mitchison, Contemporary Physics **60**, 164–187 (2019).

[36] H. E. D. Scovil and E. O. Schulz-DuBois, Phys. Rev. Lett. **2**, 262 (1959).

[37] A. Levy and R. Kosloff, Physical review letters **108**, 070604 (2012).

[38] D. Venturelli, R. Fazio, and V. Giovannetti, Phys. Rev. Lett. **110**, 256801 (2013).

[39] L. A. Correa, J. P. Palao, D. Alonso, and G. Adesso, Scientific reports **4**, 3949 (2014).

[40] P. P. Hofer, J.-R. Souquet, and A. A. Clerk, Phys. Rev. B **93**, 041418 (2016).

[41] D. Gelbwaser-Klimovsky, R. Alicki, and G. Kurizki, Phys. Rev. E **87**, 012140 (2013).

[42] P. Strasberg, C. W. Wächtler, and G. Schaller, Phys. Rev. Lett. **126**, 180605 (2021).

[43] W. Niedenzu, M. Huber, and E. Boukobza, Quantum **3**, 195 (2019).

[44] J. B. Brask, G. Haack, N. Brunner, and M. Huber, New Journal of Physics **17**, 113029 (2015).

[45] P. Erker, M. T. Mitchison, R. Silva, M. P. Woods, N. Brunner, and M. Huber, Phys. Rev. X **7**, 031022 (2017).

[46] E. Schwarzhans, M. P. E. Lock, P. Erker, N. Friis, and M. Huber, Phys. Rev. X **11**, 011046 (2021).

[47] M. P. Woods, Quantum **5**, 381 (2021).

[48] P. P. Hofer, J. B. Brask, M. Perarnau-Llobet, and N. Brunner, Phys. Rev. Lett. **119**, 090603 (2017).

[49] J. A. M. Guzmán, P. Erker, S. Gasparinetti, M. Huber, and N. Y. Halpern, Divincenzo-like criteria for autonomous quantum machines (2023), arXiv:2307.08739 [quant-ph].

[50] G. Maslennikov, S. Ding, R. Hablützel, J. Gan, A. Roulet, S. Nimmrichter, J. Dai, V. Scarani, and D. Matsukevich, Nature Communications **10**, 10.1038/s41467-018-08090-0 (2019).

[51] M. A. Aamir, P. J. Suria, J. A. M. Guzmán, C. Castillo-Moreno, J. M. Epstein, N. Y. Halpern, and S. Gasparinetti, Thermally driven quantum refrigerator autonomously resets superconducting qubit (2023), arXiv:2305.16710 [quant-ph].

[52] M. P. Woods and M. Horodecki, Physical Review X **13**, 10.1103/physrevx.13.011016 (2023).

[53] P. P. Hofer, M. Perarnau-Llobet, L. D. M. Miranda, G. Haack, R. Silva, J. B. Brask, and N. Brunner, New Journal of Physics **19**, 123037 (2017).

[54] R. C. Tolman and P. C. Fine, Rev. Mod. Phys. **20**, 51 (1948).

[55] G. T. Landi and M. Paternostro, Reviews of Modern Physics **93**, 10.1103/revmodphys.93.035008 (2021).

[56] J. M. Horowitz and T. R. Gingrich, Physical Review E **96**, 10.1103/physreve.96.020103 (2017).

[57] A. C. Barato and U. Seifert, Physical review letters **114**, 158101 (2015).

[58] G. Falasco, M. Esposito, and J.-C. Delvenne, New Journal of Physics **22**, 053046 (2020).

[59] N. Shiraishi, K. Funo, and K. Saito, Physical Review Letters **121**, 10.1103/physrevlett.121.070601 (2018).

[60] D. Janzing, P. Wocjan, R. Zeier, R. Geiss, and T. Beth, Int. J. Theor. Phys. **39**, 2717 (2000).

[61] W. S. McCulloch and W. Pitts, The bulletin of mathematical biophysics **5**, 115 (1943).

[62] F. Rosenblatt, *The perceptron, a perceiving and recognizing automaton Project Para* (Cornell Aeronautical Laboratory, 1957).

[63] I. Goodfellow, Y. Bengio, and A. Courville, *Deep Learning*

(MIT Press, 2016) http://www.deeplearningbook.org.

[64] K. Hornik, M. Stinchcombe, and H. White, Neural networks **2**, 359 (1989).

[65] D. E. Rumelhart, G. E. Hinton, and R. J. Williams, nature **323**, 533 (1986).

[66] D. P. Kingma and J. Ba, Adam: A method for stochastic optimization (2017), arXiv:1412.6980 [cs.LG].

[67] R. Ruskov and C. Tahan, Phys. Rev. B **88**, 064308 (2013).

[68] S. R. Sklan, AIP Advances **5**, https://doi.org/10.1063/1.4919584 (2015).

[69] M.-A. Lemonde, S. Meesala, A. Sipahigil, M. J. A. Schuetz, M. D. Lukin, M. Loncar, and P. Rabl, Phys. Rev. Lett. **120**, 213603 (2018).

[70] M. V. Gustafsson, T. Aref, A. F. Kockum, M. K. Ekström, G. Johansson, and P. Delsing, Science **346**, 207 (2014).

[71] W. Chen, Y. Lu, S. Zhang, K. Zhang, G. Huang, M. Qiao, X. Su, J. Zhang, J.-N. Zhang, L. Banchi, *et al.*, Nature Physics , 1 (2023).

[72] S. A. Wolf, A. Y. Chtchelkanova, and D. M. Treger, IBM journal of research and development **50**, 101 (2006).

[73] A. Mahmoud, F. Ciubotaru, F. Vanderveken, A. V. Chumak, S. Hamdioui, C. Adelmann, and S. Cotofana, Journal of Applied Physics **128**, https://doi.org/10.1063/5.0019328 (2020).

[74] S. K. Kim, G. S. Beach, K.-J. Lee, T. Ono, T. Rasing, and H. Yang, Nature materials **21**, 24 (2022).

[75] C. Z. Pratt, K. J. Ray, and J. P. Crutchfield, Dynamical computing on the nanoscale: Superconducting circuits for thermodynamically-efficient classical information processing (2023), arXiv:2307.01926 [cond-mat.stat-mech].

[76] P. Skrzypczyk, R. Silva, and N. Brunner, Phys. Rev. E **91**, 052133 (2015).

[77] P. Lipka-Bartosik and P. Skrzypczyk, Phys. Rev. X **11**, 011061 (2021).

[78] R. Silva, G. Manzano, P. Skrzypczyk, and N. Brunner, Phys. Rev. E **94**, 032120 (2016).

[79] A. Usui, W. Niedenzu, and M. Huber, Phys. Rev. A **104**, 042224 (2021).

[80] F. Clivaz, R. Silva, G. Haack, J. B. Brask, N. Brunner, and M. Huber, Phys. Rev. Lett. **123**, 170605 (2019).

[81] U. Seifert, Annual Review of Condensed Matter Physics **10**, 171 (2019).

[82] H. Wang, Nature **620**, 731 (2023).

[83] D. Venturelli, R. Fazio, and V. Giovannetti, Phys. Rev. Lett. **110**, 256801 (2013).

[84] S. Ciliberto, Phys. Rev. X **7**, 021051 (2017)

Appendix A: Details of the thermal NOT gate

The finite output rezervoir $\mathcal{B}_z$ is initialised at some temperature $\beta_z(0)$ which changes according to Eq. (15). The total heat current that flows into this reservoir is a sum of two components, i.e. the currents given by Eqs. (12) and (14). More explicitly, the respective currents are given by

$$j_{\mathcal{C}} = \mu \epsilon_z \left[g_z(\beta_z(t)) - g_z(\beta_v) \right], \tag{A1}$$

$$j_{\mathcal{M}} = \mu' \epsilon_z \left[g_z(\beta_z(t)) - g_z(\beta_r) \right], \tag{A2}$$

After a sufficiently long time, the finite rezervoir $\mathcal{B}_z$ reaches the steady-state when $\dot{\beta}_z(t) = 0$, which happens precisely when

$$g_z(\beta_z^\infty) = \Delta g_z(\beta_v) + (1 - \Delta) g_z(\beta_r), \tag{A3}$$

where $\Delta := \mu/(\mu + \mu')$ and β_z^∞ denotes the stationary value of $\beta_z(t)$. Eq. (A3) can be solved explicitly for β_z^∞, i.e.

$$\beta_z^\infty = \frac{1}{\epsilon_z} \log \left[\frac{1}{\Delta g_z(\beta_v) + (1 - \Delta) g_z(\beta_r)} - 1 \right]. \tag{A4}$$

Let us now restrict it β_z^∞ to the range $[\beta_{\min}, \beta_{\max}]$ so that it can be interpreted as a logical signal. For that we enforce the additional constraints

$$\lim_{\beta_v \to \infty} g_z(\beta_z^\infty) = g_z(\beta_{\min}), \qquad \lim_{\beta_v \to -\infty} g_z(\beta_z^\infty) = g_z(\beta_{\max}), \tag{A5}$$

where we recall that $\beta_z^\infty = \beta_z^\infty(\beta_v, \beta_r, \Delta, \epsilon_z)$ and $\beta_v = \beta_v(\beta_0, \beta_1, \epsilon_z)$. The additional requirements from Eq. (A5) lead to the following set of equations.

$$\Delta + (1 - \Delta) g_z(\beta_r) = g_z(\beta_{\min}), \tag{A6}$$

$$(1 - \Delta) g_z(\beta_r) = g_z(\beta_{\max}), \tag{A7}$$

where $g_z(\beta_{\min}) \geq g_z(\beta_{\max})$. Solving these equations with substitution $\kappa := g_z(\beta_{\min}) - g_z(\beta_{\max}) \geq 0$ leads to $\Delta = (1 - \kappa)/\kappa$ and $g_z(\beta_r) = g_z(\beta_{\max})/(1 - \kappa)$, or more precisely $\beta_r = \epsilon_z^{-1} \log[(1 - \kappa)e^{\beta_{\max}\epsilon} - \kappa]$. Plugging these values into Eq. (A4) and solving for β_z^∞ yields

$$\beta_z^\infty = \frac{1}{\epsilon_z} \log \left[\frac{1}{g_z(\beta_{\max}) + g_z(\beta_v)\kappa} - 1 \right]. \tag{A8}$$
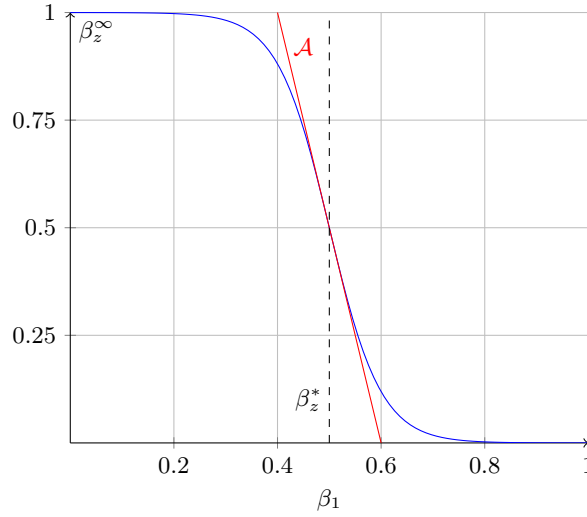
FIG. 7. The response $\beta_z^\infty(\beta_1)$ of the machine as a function of the input temperature β_1. The plot was generated using the following values of parameters: $\epsilon_z = 0.5$, $\epsilon_0 = 20$, $\beta_0 = 0.5$, $\beta_{\min} = 0$, $\beta_{\max} = 1$.

The above equation describes the steady-state response of our inverter for input β_1. We plotted β_z^∞ as a function of the input temperature β_1 for the exemplary parameters in Fig. 7.

The model has three free parameters that quantify its behaviour, namely ϵ_0, β_0 and ϵ_z. This parameters enter Eq. (A8) through the virtual temperature β_v. In order to characterize the behavior of our machine we now determine some properties of the response β_z^∞ as given by Eq. (A8). The threshold value β_z^* can be computed by finding the root of $\partial_{\beta_1}^2 \beta_z^\infty = 0$, i.e. $\beta_z^* := \arg_{\beta_1}\left(\partial_{\beta_1}^2 \beta_z^\infty = 0\right)$, which gives

$$\beta_z^* = \beta_0\left(1 + \frac{\epsilon_z}{\epsilon_0}\right) + \frac{1}{2\epsilon_0}\log\left[\frac{1 + \cosh\left(\beta_{\min}\epsilon_z\right)}{1 + \cosh\left(\beta_{\max}\epsilon_z\right)}\right]. \tag{A9}$$

For small ϵ_z we have that $\beta_z^* \approx \beta_0$, therefore in this regime β_0 specifies the threshold temperature for which the machine changes its regime of operation. Another interesting characteristic of the function β_z^∞ is the slope $\mathcal{A}$ at the threshold point, i.e.

$$\mathcal{A} := \left.\frac{\partial \beta_z^\infty}{\partial \beta_1}\right|_{\beta_1 = \beta_z^*} = -\frac{\epsilon_0}{e_z} \cdot \frac{g_{\max} + g_{\min} - 2g_{\max}g_{\min} + 2(1 - g_{\min})g_{\min}\sqrt{\frac{g_{\max}(1 - g_{\max})}{g_{\min}(1 - g_{\min})}}}{g_{\max} - g_{\min}}, \tag{A10}$$

where we used a short-hand notation $g_{\max} := g_z(\beta_{\max})$ and $g_{\min} := g_z(\beta_{\min})$. For example, for a particular choice of parameters $\beta_{\min} = 0$ and $\beta_{\max} = 1$ we have $\mathcal{A} = -(\epsilon_0/e_z)\tanh(\epsilon_z/4) = -\epsilon_0/4 + \mathcal{O}(\epsilon_z^2)$. We therefore see that, for small ϵ_z, the parameter ϵ_0 specifies the slope of the threshold in β_z^∞.

Appendix B: Details of the thermodynamic neuron model

Consider the $n + 1$ qubits $\mathcal{C}_i$ for $i \in \{0, 1, \ldots n\}$ that comprise the collector $\mathcal{C}$ with energies arranged in a vector $\boldsymbol{\epsilon} = (\epsilon_0, \epsilon_1, \ldots \epsilon_n)$ and weakly coupled to heat baths with corresponding temperatures β_i arranged in a vector $\boldsymbol{b} = (\beta_0, \beta_1, \ldots, \beta_n)$. The logical action of the thermodynamic neuron is characterized by a string $\boldsymbol{s}$ with elements ± 1 defined as $\boldsymbol{s} := [(-1)^{h_0 \oplus 1}, (-1)^{h_1 \oplus 1}, \ldots, (-1)^{h_n \oplus 1}]$. The energy of qubit $\mathcal{C}_z$ is chosen to be $\epsilon_z = (\boldsymbol{s} - \bar{\boldsymbol{s}}) \cdot \boldsymbol{\epsilon} = \sum_k (-1)^{h_k} \epsilon_k$. The steady state solution for β_z^∞ satisfies

$$g_z(\beta_z^\infty) = \Delta g_z(\beta_v) + (1 - \Delta)g_z(\beta_r), \tag{B1}$$

The virtual temperature β_v satisfies

$$e^{-\beta_v \epsilon_z} = \frac{g_0(h_0)g_1(h_1)\ldots g_n(h_n)}{g_0(h_0 \oplus 1)g_1(h_1 \oplus 1)\ldots g_n(h_n \oplus 1)} \implies \beta_v = \frac{1}{\epsilon_z}\sum_{i=0}^n \log\left[\frac{g_i(h_k \oplus 1)}{g_i(h_k)}\right] = \frac{1}{\epsilon_z}\sum_{k=0}^n (-1)^{h_k}\beta_k \epsilon_k. \tag{B2}$$

Proceeding as in Appendix A we can now restrict the range of β_z to $[\beta_{\min}, \beta_{\max}]$ by demanding that Eq. (A5) is satisfied, remembering that now β_v is a linear combination of $n+1$ temperatures. We therefore arrive at the following expression for β_z^∞:

$$\beta_z^\infty = \frac{1}{\epsilon_z} \log \left[Q(\beta_v)^{-1} - 1 \right], \tag{B3}$$

where $Q(\beta_v) := g_z(\beta_{\mathrm{hot}})g_z(\beta_v) + g_z(\beta_{\mathrm{cold}})(1 - g_z(\beta_v))$ and β_v is the virtual temperature given in Eq. (11). From here one can perform similar types of calculations as in Appendix A.